

Characterization of ammonia two-photon laser-induced fluorescence for gas-phase diagnostics

Christian Brackmann · Odd Hole · Bo Zhou ·
Zhongshan S. Li · Marcus Aldén

Received: 4 February 2013 / Accepted: 28 June 2013 / Published online: 17 July 2013
© Springer-Verlag Berlin Heidelberg 2013

Abstract Two-photon laser-induced fluorescence (LIF) of ammonia (NH_3) with excitation of the $C'-X$ transition at 304.8 nm and fluorescence detection in the 565 nm $C'-A$ band has been investigated, targeting combustion diagnostics. The impact of laser irradiance, temperature, and pressure has been studied, and simulation of NH_3 -spectra, fitted to experimental data, facilitated interpretation of the results. The LIF-signal showed quadratic dependence on laser irradiance up to 2 GW/cm^2 . Stimulated emission, resulting in loss of excited molecules, is induced above 10 GW/cm^2 , i.e., above irradiances attainable for LIF imaging. Maximum LIF-signal was obtained for excitation at the 304.8 nm bandhead; however, lower temperature sensitivity over the range 400–700 K can be obtained probing lines around 304.9 nm. A decrease in fluorescence signal was observed with pressure up to 5 bar absolute and attributed to collisional quenching. A detection limit of 800 ppm, at signal-to-noise ratio 1.5, was identified for single-shot LIF imaging over an area of centimeter scale, whereas for single-point measurements, the technique shows potential for sub-ppm detection. Moreover, high-quality NH_3 -imaging has been achieved in laminar and turbulent premixed flames. Altogether, two-photon fluorescence provides a useful tool for imaging NH_3 -detection in combustion diagnostics.

1 Introduction

With increasing awareness of the limited resources of fossil fuels, renewable biomass-derived alternatives have gained interest and an extended use of biomass energy is predicted for the future [1, 2]. This development makes ammonia (NH_3) a species of increasing relevance in combustion since it is a key species in the chemistry of fuel-bound nitrogen, of importance for combustion of many biomass fuels [3–5]. Ammonia also has potential as a hydrogen-carrier transportation fuel, allowing for combustion without carbon-containing emissions [6, 7]. Furthermore, NH_3 is used as an agent in catalytic and non-catalytic reduction of nitric oxides (NO_x) in combustion emission control [8].

Detailed understanding and optimization of combustion processes in terms of efficiency and minimization of pollutant emissions require powerful measurement techniques for characterization. The increasing role of NH_3 in combustion outlined above clearly makes techniques for its detection of high interest. Laser-based diagnostic methods, developed and applied during the last decades, enable non-invasive in situ measurements of combustion-relevant parameters such as flow velocities and temperature, as well as detection of relevant species [9]. Among the methods available for species detection, laser-induced fluorescence (LIF) based on resonant absorption of laser photons and detection of spontaneously emitted fluorescence has been widely used. Numerous species of combustion interest, including fuels or fuel tracers, intermediate species, and products can be probed using LIF, for many cases with high sensitivity and in imaging measurements.

Several alternatives exist for optical detection of NH_3 , for example line-of-sight absorption probing vibrational transitions in the infrared regime around $10 \mu\text{m}$ [10–12]. The electronic resonances of NH_3 are accessible at

C. Brackmann (✉) · O. Hole · B. Zhou · Z. S. Li · M. Aldén
Division of Combustion Physics, Lund University, Box 118,
221 00 Lund, Sweden
e-mail: christian.brackmann@forbrf.lth.se

wavelengths from around 210 nm and further down into the vacuum ultraviolet (VUV) regime [13]. Although transitions in the $A \leftarrow X$ band around 210 nm can be accessed using conventional laser systems, the quantum efficiencies of fluorescence emission are too low [13, 14]. One alternative to circumvent this has been demonstrated with photofragmentation fluorescence, in which NH_3 has been detected indirectly via fluorescence from NH generated by UV laser photolysis [15]. Another solution is to probe electronic states in the VUV regime by means of two-photon LIF, based on simultaneous absorption of two laser photons. This allows for excitation wavelengths in the UV and visible regime, and problems associated with strong absorption of combustion gases in VUV regime can be avoided. Although a much weaker process than single-photon LIF, two-photon LIF is a viable detection scheme also applicable for imaging measurements.

Two-photon LIF of NH_3 has been investigated previously for excitation to the B and C' states using excitation wavelengths 303 and 305 nm, respectively [16]. The fluorescence emission from the B state detected at 720 nm was found to be about two orders of magnitude weaker than that obtained probing the C' state with fluorescence around 565 nm. Thus, for practical diagnostics, the C' state was considered to be a better alternative. The work of Westblom and Aldén [16] also includes investigations of stimulated emission, induced simultaneously with the fluorescence, and the potential for combined $\text{NH}_3/\text{OH}/\text{NO}$ measurements. Ammonia detection probing the $C' \leftarrow X$ transitions has also been demonstrated for nonlinear optical excitation schemes such as polarization spectroscopy [17] and four-wave mixing techniques [18, 19].

This paper presents more detailed studies on NH_3 two-photon LIF from the C' state for applied diagnostics in, for example, combustion. The impact of laser irradiance, temperature dependence up to 800 K, and pressure dependence up to 5 bar (a) is investigated. In addition, the power dependence of stimulated emission has been measured to determine irradiance levels where this competing process needs to be considered. Particular emphasis has been put on the feasibility to achieve single-shot NH_3 -visualization in combustion environments and estimations of achievable signal-to-noise ratios and detection limits. Moreover, high-quality planar LIF imaging of NH_3 in the reactant mixture of laminar and turbulent premixed methane–air flames is demonstrated.

2 Experimental

A combined Nd:YAG (Quanta-Ray PRO 250-10, Spectra Physics) and dye laser (Cobra Stretch-G-2400, Sirah) system operating at 10 Hz repetition rate and with 8 ns pulse

duration was used for two-photon excitation of NH_3 . The dye laser was operated using a Rhodamine 610/640 mixture prepared for optimum output at the fundamental wavelength 610 nm, which was frequency doubled to 305 nm using a BBO crystal. The maximum output pulse energy at 305 nm was 35 mJ. The laser beam was shaped into sheets of ~ 4 mm (2.3 mm FWHM) width for spectroscopic investigations and 10–20 mm width for image acquisition using different combinations of cylindrical and spherical lenses. A variable attenuator (M-935-10, Newport) was used to reduce the laser output energy for investigations of signal power dependence.

The NH_3 -fluorescence was detected with an intensified CCD camera (PI-MAX3, Princeton Instruments). For measurements of emission spectra, fluorescence was collected and focused onto the slit of a spectrometer (Acton SpectraPro 2500, grating 1,200 grooves/mm, blaze 500 nm) using two spherical lenses of focal lengths $f = 152$ mm and $f = 37$ mm, respectively. For imaging, an $f = 50$ mm objective (Nikkor $f/1.2$) or an $f = 150$ mm UV lens (B. Halle $f/2$) was mounted on the camera, depending on the measurement object, a reversing ring and extension tubes were used to obtain suitable image magnification. While continuous background was efficiently suppressed using CCD gates of 100 ns or less, scattered laser radiation was filtered using longpass filters (Schott).

Investigations of stimulated emission (SE) were made with the laser beam focused by an $f = 100$ mm spherical lens to obtain sufficiently high laser irradiance. The signal, propagating in the forward direction of the laser beam, was collected to a photo-diode (DET 10A/M, Thorlabs) using two spherical lenses, $f = 150$ mm and $f = 100$ mm, and a digital oscilloscope (Wavemaster, LeCroy) was used for data acquisition. The UV laser radiation was suppressed using a glass plate combined with a longpass filter (GG475, Schott), and efficient suppression was assured by background measurements in pure nitrogen.

Investigations of the dependence on laser irradiance and pressure for NH_3 two-photon LIF and SE were carried out in a 200 cm^3 aluminum cell with 50 mm fused silica windows mounted. The investigations at elevated pressure were made up to 5 bar (a). Measurements at elevated temperature were made using a smaller insulated stainless steel cell, volume 8 cm^3 , with a thermocouple type K mounted inside. Excitation scan and fluorescence spectra were acquired at temperatures 295, 383, 468, 580, 675, and 780 K.

Imaging LIF measurements were made in premixed methane–air flames with NH_3 seeded to the fuel–air mixture. A conical water-cooled stainless steel Bunsen-type burner was used for NH_3 -visualization in laminar flames of equivalence ratio $\Phi = 1.3$ seeded with NH_3 -concentrations in the range 2,000–12,000 ppm. In addition, burners

consisting of water-cooled porous bronze plugs with central holes of 2 and 10 mm diameter were used. Separate supplies of fuel–air mixtures to the plug and the central hole allow for two flames to be stabilized simultaneously on this type of burner, and a conical flame stabilized on the central hole is shielded by the surrounding flame burning on the porous plug, allowing for a well-defined inner flame. The burner with the 10-mm central hole was used for measurements in laminar flames of equivalence ratio $\Phi = 0.6$ seeded with NH_3 -concentrations in the range 100–3,000 ppm. The burner with the 2-mm hole was used for measurements in laminar and turbulent flames at stoichiometric conditions with an NH_3 -concentration of 2 %. For the laminar flame, the flows of NH_3 , methane, and air were 0.04, 0.16, and 1.7 l/min, respectively, resulting in a flow speed of 10 m/s and a Reynolds number around 1400. The turbulent flame was supplied with 0.32 l/min NH_3 , 1.3 l/min methane, and 13.5 l/min air, resulting in a flow speed of 80 m/s and a Reynolds number around 11000. Methane, air, and ammonia were supplied to the burners using mass flow controllers (Bronkhorst).

To relate the NH_3 visualized in flames to the overall flame structure, simultaneous CH LIF measurements, using a previously published method [20], were carried out in the stoichiometric laminar and turbulent flames on the plug burner. Briefly, the second harmonic of a linear cavity Alexandrite laser (101-PAL, Light Age Inc.) [21] was tuned to 383.3 nm for CH excitation. The laser repetition rate was 10 Hz, the pulse duration typically 70 ns, the laser linewidth around 2.5/cm, and the output pulse energy about 80 mJ.

To facilitate interpretation of the experimental results, a simulation of the probed $C'-X v' = 2 \leftarrow v'' = 0$ electronic band was implemented using the PGOPHER software [22]. Ammonia rotational constants obtained from literature [23, 24] were adopted as initial values to fit to the experimental data. In addition, a linewidth parameter in PGOPHER was set to 0.089/cm in order to fit the overall contour of the spectra.

3 Results and discussion

3.1 NH_3 spectroscopy

The energy-level diagram depicted in Fig. 1a outlines the probed $C'-X v' = 2 \leftarrow v'' = 0$ transition at 304.8 nm, identified in previous investigations as the one giving strongest fluorescence emission and having the greatest potential for diagnostics [16]. Excitation scan and fluorescence spectra, acquired at room temperature and atmospheric pressure, are presented in Fig. 1b, c, respectively. The excitation scan (Fig. 1b) shows overlapping

ro-vibrational transitions in the $C'-X$ band mainly from the qQ-branch, with the bandhead at 304.8 nm being the most prominent feature. The fluorescence emission spectrum (Fig. 1c) covers a range of typically 10 nm containing multiple rotational transitions of qP, qQ, and qR branches [23]. Even though the spectrum was measured with a spectral resolution of around 0.25 nm, a rather smooth shape without distinct features is observed. This is attributed to the short effective lifetimes of the pre-dissociative C' - and A -states, resulting in rather broad spectral lines

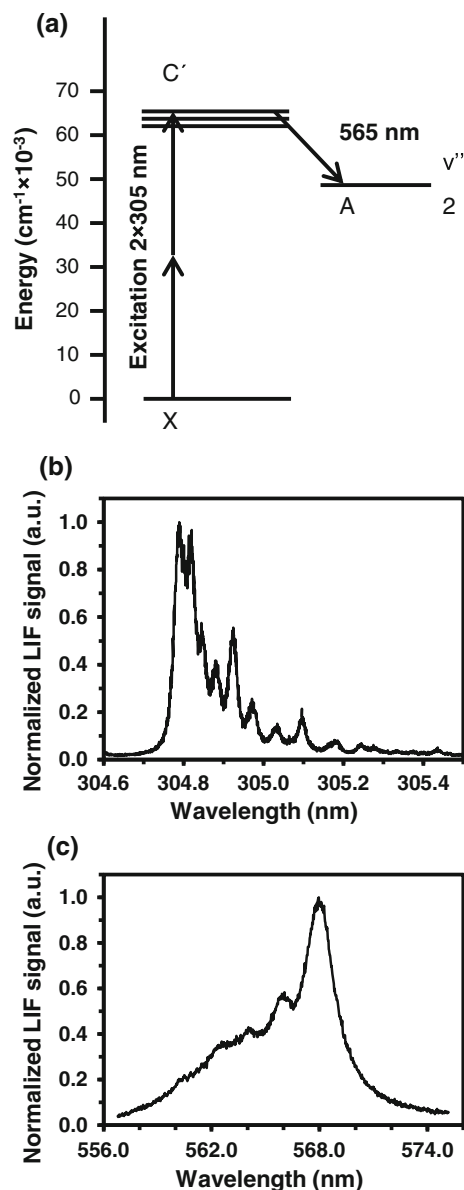


Fig. 1 a Schematic energy-level diagram indicating the probed $C' \leftarrow X$ and $C' \rightarrow A$ transitions of NH_3 . b $C'-X v' = 2 \leftarrow v'' = 0$ excitation scan acquired at 295 K and atmospheric pressure. The identifiable lines mainly consist of overlapping qQ-branch rotational lines. c $C'-A v' = 2 \rightarrow v'' = 2$ fluorescence emission spectrum at 295 K and atmospheric pressure

[23]. Effective lifetimes of 6.1 and 0.1 ps have been reported for the NH_3 C' - and A -states, respectively [25, 26].

3.2 Power dependence investigations

Since relatively high laser irradiance is necessary for two-photon excitation and the NH_3 excitation scheme involves pre-dissociative molecular states, characterization of the NH_3 LIF-signal power dependence is required. Figure 2 shows power dependence data measured at room temperature and atmospheric pressure with the beam focused into a $2.3 \text{ mm} \times 0.1 \text{ mm}$ laser sheet, thus tighter than for a typical LIF imaging setup but not enough to reach irradiances where stimulated emission can be induced. This can be seen by comparison with the stimulated emission data presented in the same graph and acquired with the beam focused into a $100\text{-}\mu\text{m}$ -diameter spot using an $f = 100 \text{ mm}$ spherical lens. The LIF data essentially follows an I^2 dependence also reported for two-photon excitation of $A \leftarrow X$ transitions of ND_3 [27]. A deviation of around 10 % toward a weaker dependence can be observed at the highest irradiances, typically above 1 GW/cm^2 . The reduced power dependence could be explained by enhanced two-photon absorption of the laser beam when passing through NH_3 prior to the probe volume in the center of the cell. Another possibility is increased loss of excited NH_3 molecules due to ionization. The stimulated emission signal started to be detectable at laser irradiance around 10 GW/cm^2 and shows a highly nonlinear I^5 power dependence. As the SE is induced only at high irradiances, it does not compose a loss mechanism for two-photon NH_3 fluorescence imaging performed at lower laser irradiances. Nevertheless, it needs to be considered for single-point measurements using a focused beam, as reported by Westblom and Aldén [16], especially when aiming to detect low NH_3 -concentrations.

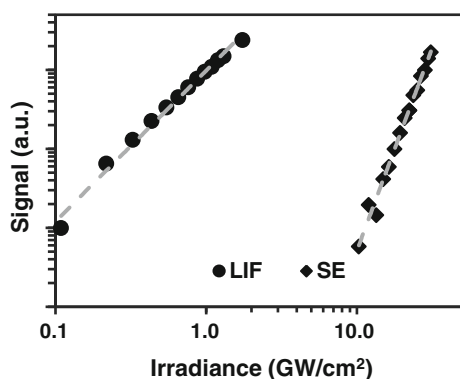


Fig. 2 Power dependence plots of NH_3 two-photon laser-induced fluorescence (LIF) and stimulated emission (SE) data measured at ambient conditions. The LIF and SE data follow I^2 and I^5 dependencies, respectively

3.3 Temperature dependence

Accurate fluorescence imaging of NH_3 -distributions requires knowledge of the LIF-signal temperature dependence, and investigations of this are summarized in Fig. 3. Figure 3a, b shows excitation scan spectra measured in NH_3 at temperatures 383 and 780 K, respectively. In addition to the measured data, spectra simulated using PGOPHER are also included together with profiles of the residuals between simulations and experimental data. The molecular parameters used for spectral simulation are presented in Table 1 together with corresponding data from literature. The residuals indicate a shift between peaks of

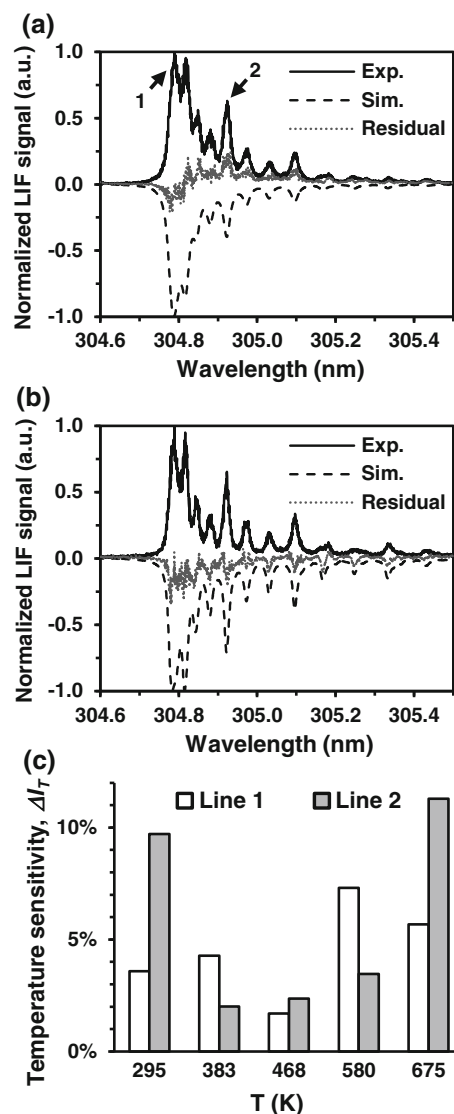


Fig. 3 Experimental (solid) and simulated (dashed) NH_3 LIF excitation scan spectra with residuals (dotted gray). **a** 383 K. **b** 780 K. **c** NH_3 LIF temperature sensitivity for lines 1 and 2, indicated in (a), calculated as the percentage change in LIF-signal. Details are given in Results Sect. 3.3

Table 1 NH₃ rotational constants from fit of experimental data using the PGOPHER software

Constant	PGOPHER fit (cm ⁻¹)	Ashfold et al. [23] (cm ⁻¹)	Nolde et al. [24] (cm ⁻¹)
Band origin	65,598.16	63,865.62 (<i>v</i> = 0) 64,709.49 (<i>v</i> = 1)	63,866.397 (0.028) (<i>v</i> = 0) 64,710.41 (0.05) (<i>v</i> = 1)
<i>B</i>	10.041	10.778 (<i>v</i> = 0) 10.323 (<i>v</i> = 1)	10.770 (0.001) (<i>v</i> = 0) 10.332 (0.001) (<i>v</i> = 1)
<i>C</i>	5.399	5.264 (<i>v</i> = 0) 5.322 (<i>v</i> = 1)	5.229 (0.0009) (<i>v</i> = 0) 5.281 (0.001) (<i>v</i> = 1)
10 ⁶ <i>D</i> _J	1,636.28	1,091 (<i>v</i> = 0) 416 (<i>v</i> = 1)	242 (8) (<i>v</i> = 0) -287 (8) (<i>v</i> = 1)
10 ⁶ <i>D</i> _{JK}	-2,461.72	-2,043 (<i>v</i> = 0) -541 (<i>v</i> = 1)	-588 (12) (<i>v</i> = 0) 744 (9) (<i>v</i> = 1)
10 ⁶ <i>D</i> _K	866.94	910 (<i>v</i> = 0) 36 (<i>v</i> = 1)	211 (15) (<i>v</i> = 0) 607 (11) (<i>v</i> = 1)

experimental data and simulated spectra. Nevertheless, simulations show qualitative agreement with experimental data and allow for reliable identification of the transitions corresponding to the spectral lines. Molecular constants of the high-order terms in the calculations of rotational energy were not included in the present PGOPHER model and may explain the observed difference between the experimental data and spectral simulation.

Clearly, excitation at the wavelength giving strongest signal is beneficial for efficient NH₃-detection. However, to facilitate interpretation of NH₃ LIF-signals from combustion environments, where temperature in the measurement region may vary, it is also desirable to probe energy levels with populations that have rather weak temperature dependence. Figure 3c shows results from an analysis of the temperature sensitivity for the LIF-signals averaged over spectral intervals similar to the laser linewidth and located at the peaks around 304.8 nm (line 1) and 304.9 nm (line 2) both indicated in Fig. 3a. While line 1 consists of a dense line structure of multiple transitions in the qQ-branch bandhead, line 2 is a combination of 5 overlapping qQ transitions. For data evaluation, excitation scans measured at six temperatures $T_i = 295, 383, 468, 580, 675,$ and 780 K were first normalized versus the total integrated signal in the spectrum. Factors affecting the LIF-signal that are common for the entire spectrum are cancelled by the normalization and an analysis of changes in spectral shape can be carried out. Temperature sensitivities for line 1 and 2, ΔI_{T_i} , as presented in Fig. 3c, have been calculated using the relation $\Delta I_{T_i} = \left| \frac{I_{T_{i+1}} - I_{T_i}}{I_{T_i}} \right|$, i.e., as percentage change in fluorescence signal between normalized spectra of temperatures T_i and T_{i+1} . At temperatures 295 and 675 K, line 2 shows stronger temperature dependence, sensitivity values of 10–11 %, than line 1, sensitivity values 4–6 %. Nevertheless, it can be noted that line 2, although of lower signal strength, shows better temperature stability with lower sensitivity values, 2–3 %, over the interval 400–700 K.

Thus, in order to minimize temperature sensitivity and enable correct qualitative and quantitative fluorescence measurements, line 2 seems the preferable excitation alternative.

Measurements of NH₃ and temperature in premixed methane–air flames, with NH₃ seeded into the fuel (data not shown), show that it is typically consumed at temperatures below 800 K. Moreover, the operating temperature interval for catalytic NO_x reduction using ammonia is generally 500–800 K [28]. Thus, the investigated temperature interval is relevant for combustion with ammonia as fuel component as well as for catalytic reduction. Non-catalytic thermal reduction is typically induced at higher temperatures, 1,000–1,300 K [28–30], outside the range of the acquired data. However, spectral simulations using the developed PGOPHER model suggest an overall signal decrease by a factor of 2.5–3 compared with 300 K. In addition at these higher temperatures, the relative strength of spectral line 2 approaches that of line 1. Thus, ammonia detection by two-photon fluorescence should also be feasible at higher temperature, provided that the chemical conditions are such that it remains stable. For example, the auto-ignition temperature for ammonia in air is 924 K [31].

3.4 Pressure dependence

The increase in molecular number density and number of NH₃-molecules in the LIF probe volume with pressure would in principle enhance the NH₃ LIF-signal. However, elevated pressure also introduces spectral line broadening and influences competing processes such as collisional quenching, photo-dissociation, and SE. The pressure dependence of the NH₃ LIF-signal is thus a combined effect of these phenomena.

Figure 4 presents results from measurements in pure NH₃ up to an absolute pressure of 5 bar. Spectral line

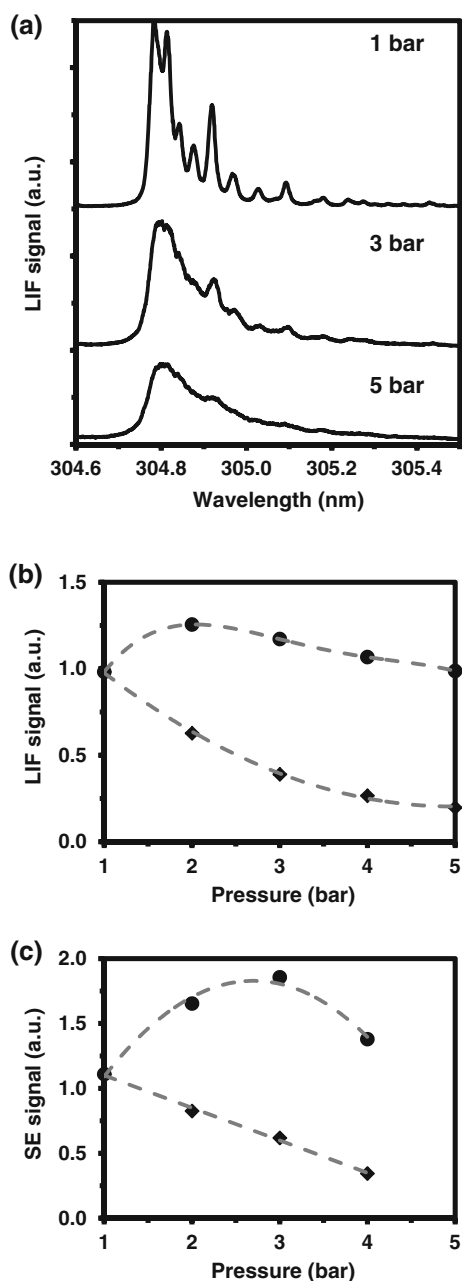


Fig. 4 **a** NH₃ excitation scan spectra for pressures 1, 3, and 5 bar. Spectra show an increased line broadening with pressure resulting in a decrease in peak signal strength. **b** Integrated LIF-signal versus pressure. **c** SE signal versus pressure. Data are shown with (diamonds) and without (circles) normalization versus pressure; dashed curves are inserted as guidance for the reader

broadening induced at elevated pressure is displayed in the excitation scan spectra of Fig. 4a in which structures are still visible at a pressure of 3 bar whereas at 5 bar the spectrum essentially consists of a single broad feature. For excitation of NH₃ at a fixed wavelength position such as line 1 (indicated in Fig. 3a), the broadening results in reduced overlap between the spectral profile of the laser and the NH₃-spectrum resulting in significant signal reduction.

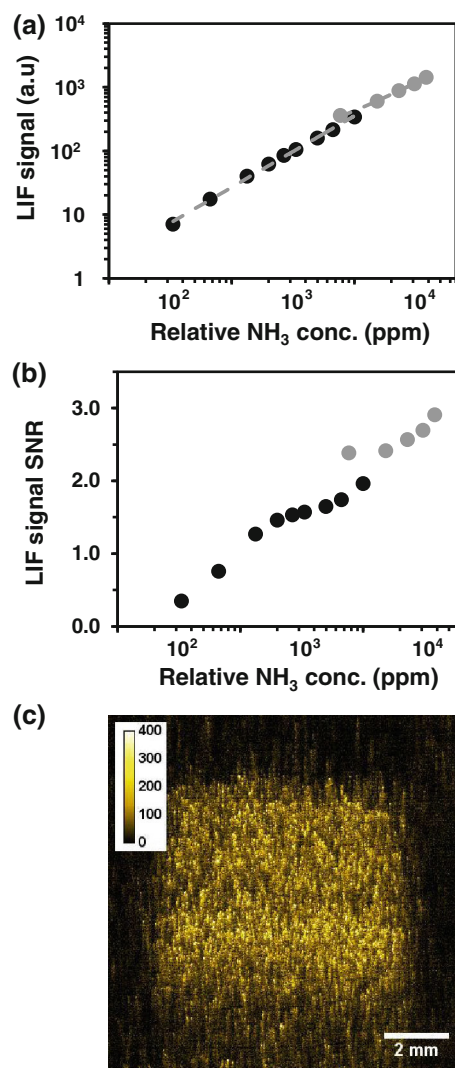


Fig. 5 NH₃ LIF-signal versus relative NH₃-concentration in the reactant NH₃-methane-air mixture of premixed laminar flames. **a** Average single-shot image LIF-signal, showing a linear dependence on concentration. **b** Signal-to-noise ratio (SNR), defined as the ratio between average single-shot image signal and standard deviation. **c** Single-shot LIF image obtained at concentration 800 ppm, SNR 1.5

The impact of other effects than line broadening can be observed studying the integrated LIF-signal of excitation scan spectra, and this is plotted versus pressure in Fig. 4b. Without normalization versus pressure, the signal (circles) shows an increase up to 2 bar, due to a higher volume number density of the gas, followed by a decrease toward higher pressures. When normalized versus pressure, the integrated LIF-signal shows a decreasing trend over the entire pressure range as shown in Fig. 4b (diamonds), indicating a pressure-dependent fluorescence loss mechanism. Losses due to SE can most likely be excluded since measurements were made at laser irradiance levels below the identified threshold for simulated emission shown in Fig. 2. Additionally, measurements of stimulated emission

versus pressure, data shown in Fig. 4c, show trends similar to those of LIF with a decrease in signal versus pressure. Even though the C' state of NH_3 is pre-dissociative, the clear decrease in fluorescence observed with increasing pressure suggests another loss mechanism than dissociation, for which a generally rather weak dependence on pressure has been reported [32]. The results suggest that the NH_3 LIF-signal is reduced at elevated pressure due to collisional quenching, and it is possible that dissociation is not the totally dominating loss mechanism. Thus, collisional quenching could have a substantial impact on NH_3 -fluorescence, an issue which merits further investigations. In particular, characterization of NH_3 -detection at elevated pressure is relevant due to the potential of NH_3 as a fuel for internal combustion engines [7, 33].

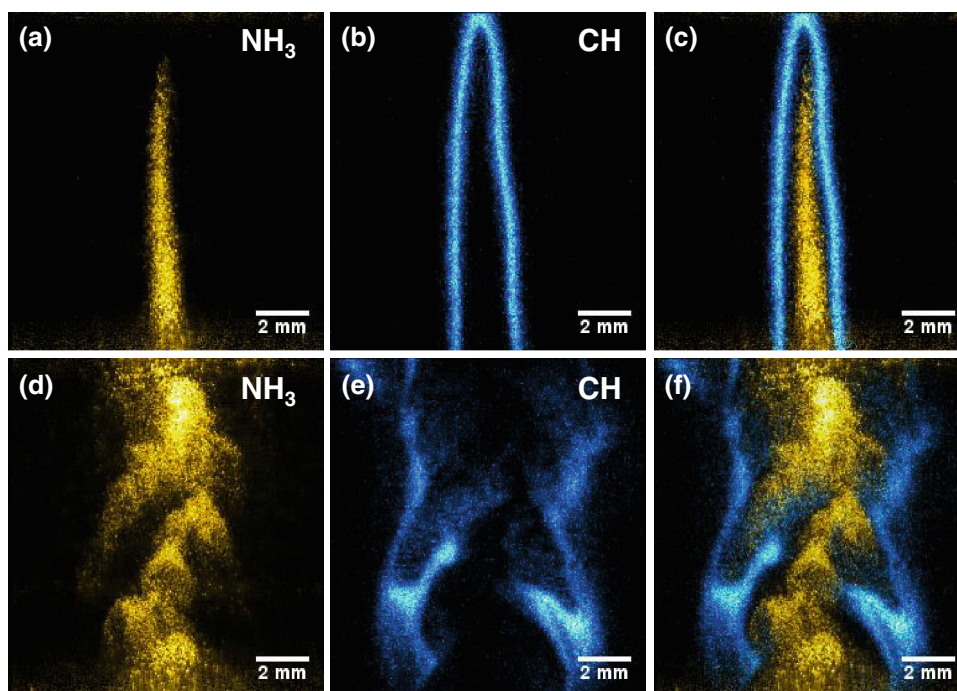
3.5 Fluorescence imaging

Results from evaluation of single-shot NH_3 LIF imaging are presented in Fig. 5. Figure 5a shows two data sets of signal versus relative NH_3 -concentrations measured in NH_3 -methane-air mixtures burning in premixed laminar flames. Both data sets were measured with laser pulse energy around 35 mJ, and the effective laser sheet widths for NH_3 -excitation regions were 10–11 mm. A linear relation between the signal and amount of NH_3 can be observed for all data. The ratio between average NH_3 -signal and the standard deviation between single-shot images, the signal-to-noise ratio (SNR), is plotted versus relative NH_3 -concentration in Fig. 5b, and a value of ~ 1.5

is obtained at a concentration around 800 ppm. The standard deviation values squared and the corresponding average NH_3 -signal values squared can be fitted to a second-order polynomial, in agreement with noise characteristics reported for intensified CCD cameras [34]. The SNR data sets partially overlap at concentrations above 2,000 ppm; nevertheless, the data points belonging to the set continuing at higher concentrations (gray circles) show higher signal-to-noise ratio. However, for this data set, the imaged NH_3 -region was sampled over a lower number of pixels, 200 in the vertical direction, most likely explaining the observed offset. A sample single-shot image acquired at an NH_3 -concentration of 800 ppm is shown in Fig. 5c. The image spatial resolution is 0.026 mm/pixel, and the NH_3 -region is distributed over 350 pixels in the vertical direction. The height of the visualized NH_3 -region in Fig. 5c is 10 mm, and the laser irradiance can be estimated to 250 MW/cm². If the beam would have been focused to a point using a spherical lens, the vertical size would have been reduced by one to two orders of magnitude and the irradiance would increase correspondingly to ~ 10 GW/cm². If a quadratic dependence on laser irradiance is assumed, cf. Fig. 2, and losses due to stimulated emission are avoided, cf. Fig. 2, an improvement of the detection limit by four orders of magnitude can be expected, i.e., from thousands of ppm down to sub-ppm level under favorable conditions.

Figure 6 shows NH_3 and CH LIF images measured simultaneously in premixed laminar, Fig. 6a–c, and turbulent, Fig. 6d–f, stoichiometric NH_3 -methane-air flames

Fig. 6 Corresponding single-shot NH_3 and CH LIF images, simultaneously acquired in laminar ($Re = 1,400$) (a–c) and turbulent ($Re = 11,000$) (d–f) NH_3 -methane-air flames. Flame conditions are given in the Sect. 2. Image overlays are shown in c and f. The laminar flame shows a distinct gap between the central NH_3 -cone (yellow) in the fuel-air mixture and the thin CH-cone (blue) of the flame reaction zone. This indicates NH_3 decomposition in the flame preheat zone. The turbulent flame shows a more complex pattern allowing reaction zone CH stretching into the NH_3 -region



with NH_3 -concentrations of 2 %. The CH-signal assists visualizing the flame structure, and the combined images clearly demonstrate the ability for ammonia visualization under combustion conditions with NH_3 as a fuel component. Measurements in the laminar flame were made on a well-defined unburned homogeneous NH_3 -methane-air mixture whereas in the case of turbulent combustion mixing with hot burned gases makes the situation more complex.

For CH planar LIF measurements, the addition of NH_3 to the flame resulted in an increased LIF-signal intensity as well as a broadened distribution, in particular for images acquired in the turbulent flame as shown in Fig. 6e, where the CH PLIF layer was expected to be thinner from previous observations [35, 36]. While Fig. 6 presents simultaneously acquired images, these effects on CH were also observed for separate measurements, excluding signal cross-talk and photochemical effects induced by the 304.8 nm laser used for NH_3 -excitation. Moreover, data from laminar flames show that the signals are well separated in space, as shown in Fig. 6c, with the broadening of the CH-signal located in the product zone on the outer side of the flame cone. Thus, direct signal interference from NH_3 -photolysis seems unlikely and the observed effects of NH_3 -addition on the CH-signal require further investigations. Nonetheless, it is clear that structures of the mixing of ammonia with other gases can be visualized with high image quality and fine detail. Mixing of ammonia with flue gases has been identified as a key parameter for efficient NO_x reduction [37, 38] making this kind of method a valuable tool for increased understanding and optimization of the ammonia deNO_x process.

4 Conclusions

A characterization of two-photon LIF for visualization of gas-phase NH_3 , primarily under conditions related to combustion, has been presented. Dependencies on laser irradiance, temperature, and pressure as well as the potential interference from stimulated emission have been investigated. Experimental data acquired under well-defined conditions have also been used as basis for a PGOPHER-simulation used for interpretation and further prediction of signal behavior. While the strongest LIF-signal was obtained for excitation at the $C'-X v' = 2 \leftarrow v'' = 0$ bandhead at 304.8 nm, a less temperature sensitive alternative can be obtained for excitation at 304.9 nm. Even though the C' state is reported to be pre-dissociative, a reduced signal observed with higher pressure indicates increasing influence of collisional quenching. A detection limit for LIF NH_3 -imaging, resulting in a signal-to-noise ratio of ~ 1.5 for two-dimensional visualization on a centimeter scale, has been estimated to around 800 ppm. The

obtained results suggest a detection limit at sub-ppm level for single-point measurements using a focused laser beam. Thus, two-photon fluorescence allows for sensitive, specific, single-shot detection of NH_3 under conditions relevant for combustion and especially the opportunity for imaging makes it a highly useful diagnostic tool.

Acknowledgments This work has been financed by SSF (Swedish Foundation for Strategic Research), the Swedish Energy Agency through CECOST (Centre for Combustion Science and Technology), Swedish-Chinese collaboration project (Project No. 33305-1), VR (Swedish Research Council), and the European Research Council Advanced Grant DALDECS. Odd Hole thanks for financial support provided by Scania.

References

1. M. Parikka, *Biomass Bioenergy* **27**, 613–620 (2004)
2. M. Balat, *Energy Source Part A* **31**, 1160–1173 (2009)
3. A.M. Dean, J.W. Bozzeli, in *Gas-phase Combustion Chemistry*, ed. by W. C. Gardiner Jr. (Springer, New York, 2000), pp. 125–343
4. P. Glarborg, A.D. Jensen, J.E. Johnsson, *Prog. Energy Combust.* **29**, 89–113 (2003)
5. A. Williams, J.M. Jones, L. Ma, M. Pourkashanian, *Prog. Energy Combust.* **38**, 113–137 (2012)
6. C. Duynslaegher, F. Contino, J. Vandooren, H. Jeanmart, *Combust. Flame* **159**, 2799–2805 (2012)
7. C. Duynslaegher, H. Jeanmart, J. Vandooren, *Fuel* **89**, 3540–3545 (2010)
8. L.J. Muzio, G.C. Quartucy, *Prog. Energy Combust. Sci.* **23**, 233–266 (1997)
9. K. Kohse-Höinghaus, J.B. Jeffries, in *Applied Combustion Diagnostics*, (Taylor&Francis, New York, 2002)
10. A.P. Force, D.K. Killinger, W.E. Defeo, N. Menyuk, *Appl. Optics* **24**, 2837–2841 (1985)
11. W. Meienburg, H. Neckel, J. Wolfrum, *Appl. Phys. B-Photo* **51**, 94–98 (1990)
12. W. Meienburg, J. Wolfrum, H. Neckel, *Twenty-Third Symposium on Combustion/The Combustion Institute* **23**, 231–236 (1990)
13. B.M. Cheng, H.C. Lu, H.K. Chen, M. Bahou, Y.P. Lee, A.M. Mebel, L.C. Lee, M.C. Liang, Y.L. Yung, *Astrophys. J.* **647**, 1535–1542 (2006)
14. S. Koda, P.A. Hackett, R.A. Back, *Chem. Phys. Lett.* **28**, 532–533 (1974)
15. S.G. Buckley, C.J. Damm, W.M. Vitovec, L.A. Sgro, R.F. Sawyer, C.P. Koshland, D. Lucas, *Appl. Optics* **37**, 8382–8391 (1998)
16. U. Westblom, M. Aldén, *Appl. Spectrosc.* **44**, 881–886 (1990)
17. K. Nyholm, R. Fritzon, N. Georgiev, M. Aldén, *Opt. Commun.* **114**, 76–82 (1995)
18. M.N.R. Ashfold, I.W. Chandler, C.C. Hayden, R.I. McKay, A.J.R. Heck, *Chem. Phys.* **201**, 237–244 (1995)
19. N. Georgiev, M. Aldén, *Appl. Phys. B-Photo* **56**, 281–286 (1993)
20. Z.S. Li, J. Kiefer, J. Zetterberg, M. Linvin, A. Leipertz, X.S. Bai, M. Aldén, *P Combust. Inst.* **31**, 727–735 (2007)
21. Z.S. Li, M. Afzelius, J. Zetterberg, M. Aldén, *Rev. Sci. Instrum.* **75**, 3208–3215 (2004)
22. C.M. Western, PGOPHER, A program for simulating rotational structure, (University of Bristol, Bristol, UK, 2010). <http://pgopher.chm.bris.ac.uk>

23. M.N.R. Ashfold, C.L. Bennett, R.N. Dixon, P. Fielden, H. Rieley, R.J. Stickland, *J. Mol. Spectrosc.* **117**, 216–227 (1986)
24. M. Nolde, K.M. Weitzel, C.M. Western, *Phys. Chem. Chem. Phys.* **7**, 1527–1532 (2005)
25. M.N.R. Ashfold, R.N. Dixon, N. Little, R.J. Stickland, C.M. Western, *J. Chem. Phys.* **89**, 1754–1761 (1988)
26. M.N.R. Ashfold, C.L. Bennett, R.N. Dixon, *Faraday Discuss.* **82**, 163–175 (1986)
27. M.N.R. Ashfold, C.L. Bennett, R.N. Dixon, *Chem. Phys.* **93**, 293–306 (1985)
28. M. Radojevic, *Environ. Pollut.* **102**, 685–689 (1998)
29. R.K. Lyon, *Environ. Sci. Technol.* **21**, 231–236 (1987)
30. R. Hemberger, S. Muris, K.U. Pleban, J. Wolfrum, *Combust. Flame* **99**, 660–668 (1994)
31. I. Glassman, *Combustion*, 3rd edn. (Academic Press, San Diego, 1996)
32. K. Kohse-Höinghaus, *Prog. Energy. Combust.* **20**, 203–279 (1994)
33. A.J. Reiter, S.C. Kong, *Fuel* **90**, 87–97 (2011)
34. J. McGinty, J. Requejo-Isidro, I. Munro, C.B. Talbot, P.A. Kellest, J.D. Hares, C. Dunsby, M.A.A. Neil, P.M.W. French, *J. Phys. D Appl. Phys.* **42**, 1–9 (2009)
35. J. Kiefer, Z.S. Li, J. Zetterberg, X.S. Bai, M. Aldén, *Combust. Flame* **154**, 802–818 (2008)
36. Z.S. Li, B. Li, Z.W. Sun, X.S. Bai, M. Aldén, *Combust. Flame* **157**, 1087–1096 (2010)
37. M. Østberg, K. Dam-Johansen, J.E. Johnsson, *Chem. Eng. Sci.* **52**, 2511–2525 (1997)
38. G.-W. Lee, B.-H. Shon, J.-G. Yoo, J.-H. Jung, K.-J. Oh, *J. Ind. Eng. Chem.* **14**, 457–467 (2008)